# Scattering of *s*-polarized plane waves by finite-thickness periodic structures made of ultralow-permittivity metamaterials

A. E. Serebryannikov,* T. Magath,† K. Schuenemann, and O. Y. Vasylchenko‡
*Technische Universitaet Hamburg-Harburg, D-21071 Hamburg, Germany*
(Received 29 July 2005; revised manuscript received 14 November 2005; published 17 March 2006)

Scattering of *s*-polarized plane waves by finite-thickness periodic structures is studied, which contain components made of ultralow-permittivity metamaterial (ULPM), and therefore exhibit intermediate properties between those made of pure metals and of pure dielectrics. The numerical results presented demonstrate basic frequency- and angular-selectivity-concerned effects arising in the structures with sinusoidal corrugations, which are made of ULPM, and for a stack of two such periodic structures, in which one of them is made of ULPM and the other one of a dielectric. The results presented are mostly related to the zero-permittivity case, when there is no wave propagating in the transverse direction within the metamaterial. The field inside ULPM is either close to or exactly the static one. For the structures of the first type, this can lead to a straightening of the field lines at the lower (noncorrugated) interface and, in turn, to a suppressing of higher modes (Bragg beams) in the transmitted field, which are allowed to propagate. The known property of a zero-permittivity noncorrugated slab, i.e., the cutoff-type frequency dependence of the transmittance, appears also for corrugated periodic structures studied in both single- and multimode regimes. In our study, a similar behavior vs the angle of incidence is demonstrated and a condition for its appearance is given. For the structures of the second type, it is shown that these effects can be combined with those, which are typical for dielectric gratings and usually associated with bulk and surface modes. Stacking ULPM and dielectric layers can also lead to an enhancement of some effects, which are inherent to each of the layers, as well as to several abnormal effects. The effects found promise to be useful for controlling and, in particular, for splitting/combining of light and microwave radiation.

DOI: 10.1103/PhysRevB.73.115111 PACS number(s): 42.25.Fx, 78.20.Ci, 03.50.De, 81.05.Zx

## I. INTRODUCTION

During the past years, the interest in metamaterials has grown dramatically, since they allow us to realize electromagnetic properties which are different from those of conventional metals and dielectrics. Due to this, they provide a new tool to control wave propagation from microwaves up to the visible. In fact, metamaterials are a modern extension of the concept of artificial dielectrics, which were proposed more than 50 years ago. A large number of works has recently been published concerning theoretical aspects, performance, and applications of double-negative (DNG), single-negative, double-positive, zero-permittivity, and zero- and ultralow-index metamaterials, e.g., Refs. 1–17.

Most of the studies in this field have been devoted to planar structures. In some works, structures with curvilinear boundaries, which are made of metamaterials, have also been considered. For example, scattering properties of a cylinder[18] and sphere[19] fabricated from a DNG material and a conducting cylinder coated with a DNG material,[20] and radiation from a DNG ring enclosure[21] have been studied. In Ref. 11, a circular cylinder and a sphere made of matched zero-index material has been a subject to study. Peculiarities of diffraction of a plane wave by a DNG-metamaterial half-space with corrugated boundary have been reported in Refs. 22 and 23.

Among the interesting properties revealed for a zero-index medium slab, it is worth mentioning the narrowing of the far-field pattern while a source of radiation is placed within the slab and the transforming of curved wavefronts into planar ones.[11] Zero-index/permittivity behavior is often considered to be typical for photonic crystals and for periodic structures (PS) used in the resonance regime as well and can be observed even in purely dielectric structures (e.g., see Refs. 4, 11, and 15, and references therein). The presence of a band gap is not necessary if the photonic crystal contains metallic constituents. In line with known homogenization theories and/or physical considerations, ultralow values of the effective index/permittivity can be obtained in this case by embedding metallic rods (non)periodically in a host dielectric (e.g., see Refs. 24 and 25).

A long time ago, the possibility of realizing a composite with $\mathrm{Re}\{\varepsilon_{\mathrm{eff}}\}<1$ has already been demonstrated for phase-advance artificial dielectrics which were designed for microwave applications.[26,27] Modern facilities of nanofabrication can generate sizes, which are much smaller than the visible wavelength. Therefore, a material with zero or ultralow index/permittivity can also be fabricated for applications in the optical regime. Typical geometrical dimensions of the associated structures which consist of rods arranged in a square lattice can be found, for example, in Refs. 4 and 9. It has been shown therein that the lattice constant $a$ should be at least twice as small as wavelength $\lambda$ in order to obtain zero (ultralow) index/permittivity. According to Ref. 4, zero-permittivity behavior manifests itself in total transmission through the slab near zero frequency and in arising of a wide gap in transmission between a near-zero frequency and a frequency, which is of the order of $\omega=\pi c/a$. The studies in Refs. 4 and 9 have been performed for the effectively noncorrugated structure, i.e., in a single-mode regime. Interesting zero/ultralow-index/-permittivity related effects are also

 

expected to appear in PS of various types, where they could be realized in both single- and multimode regimes.

In the present paper, we consider scattering of an *s*-polarized electromagnetic wave by a finite-thickness PS made of an ultralow-permittivity material (ULPM), to which both zero-permittivity (ZPM) and ultralow-index materials considered in Refs. 4, 8, and 9 can be assigned. We assume that $0 \leqslant \mathrm{Re}\{\varepsilon_{\mathrm{eff}}\} < 1$. Our consideration is restricted to the case of sinusoidal corrugations. It is assumed that $\lambda$ is large enough in order to provide effective homogeneity of the ULPM in the whole range of the geometrical parameters and for each frequency value used.

The aim of this work is to study the peculiarities of scattering by PS which appear due to the presence of an ULPM. PSs of two types are considered. One of them is a finite-thickness PS, entirely made of an ULPM, with boundaries corrugated on the upper and noncorrugated on the lower side, respectively. The other type is a stack of two PS, which represents a two-layer structure with noncorrugated outer boundaries and a corrugated inner boundary between a metamaterial and a dielectric layer. Emphasis in the numerical study is put on ZPM, a special case of ULPM, which corresponds to the infinite phase velocity.[12] Both frequency and angular behaviors of the far field, in both single- and multimode regimes, are studied in terms of diffraction efficiencies (DE), which characterize the energy distribution between the modes. Besides, several examples of near-field patterns are presented. The numerical results presented have been obtained with the aid of a recently developed fast coupled-integral-equations technique.[28]

## II. THEORETICAL BACKGROUND

A rod (wire) medium is commonly used to realize various effective material properties. In the case of periodically located rods made of a Drude metal one can obtain the medium which effectively behaves as an artificial plasma with permittivity[29]

$$\varepsilon_{\mathrm{eff}} = 1 - \frac{\omega_{\mathrm{eff}}^2}{\omega(\omega + i\varepsilon_0 a^2 \omega_{\mathrm{eff}}^2/\pi b^2 \sigma)}, \tag{1}$$

where $\omega_{\mathrm{eff}}^2 = 2\pi c^2/a^2 \ln(a/b)$ means the second power of effective plasma frequency, $\sigma$ is the conductivity of the metal, $b$ is the rod radius, and $\varepsilon_0$ is free-space permittivity. In turn, the dependence of $\sigma$ on $\omega$ should be taken into account, if the condition $\gamma \gg \omega$ is not satisfied,[30] where $\gamma$ is the collision frequency of the metal. $\omega_{\mathrm{eff}}$ can be much lower than the plasma frequency for a pure metal (which is typically $10^3 - 10^4$ THz) and can be scaled down to microwave frequencies.[29] According to (1), $\mathrm{Re}\{\varepsilon_{\mathrm{eff}}\} = 0$ at a certain $\omega$.

Note that $\mathrm{Re}\{\varepsilon_{\mathrm{eff}}\} = 0$ can also be obtained in disordered systems by using a proper volume fraction of metallic constituents, provided that the long-wave approximation

$$\omega \ll 2\pi c/\bar{a} \tag{2}$$

is valid for the average distance between neighboring rods $\bar{a}$. Although a plasmonic material showing $\mathrm{Re}\{\varepsilon_{\mathrm{eff}}\} = \mathrm{const}$ and $\mathrm{Im}\{\varepsilon_{\mathrm{eff}}\} = \mathrm{const}$ over a wide range of $\omega$ variation is hypothetical, its consideration is useful for revealing the basic features of transmission/reflection vs $\omega$. This fact has before been exploited in many studies devoted to the structures containing metamaterials.

In Ref. 4, the transmittance $\mathcal{T}$ through a slab of the rod medium has been studied using the simplest mixing formula $\varepsilon_{\mathrm{eff}} = f\varepsilon_m + (1-f)\varepsilon_h = 0$, where $\varepsilon_h$, $\varepsilon_m = \mathrm{const}$, and $f$ are the permittivities of the host medium and metallic inclusions, and filling fraction, respectively. Using this formula and some physical considerations, it was demonstrated in Ref. 4 that $\mathcal{T}$ has to rise to unity with $\omega$ tending to zero, while a wide gap in the frequency dependence of $\mathcal{T}$ occurs between a near zero frequency and $\omega \propto 2\pi c/a$. It can easily be shown that at least within the frequency range where Eq. (2) is valid, this behavior qualitatively coincides with that observed in the case of a noncorrugated homogeneous slab with $\varepsilon = 0$. The latter can be obtained from the standard formulas for transmission and reflection in planar homogeneous layered structures using Snell's Law (e.g., Refs. 31 and 32), where $\varepsilon$ of the slab is very close to zero. For example, the value $|\varepsilon| = 10^{-12}$ can still be used, while any further decrease of $|\varepsilon|$ does not lead to a noticeable difference in $\mathcal{T}$.

We are interested in the frequency region, where a cutoff behavior of $\mathcal{T}$ is expected to appear, i.e., $\omega_{\mathrm{cut}} \ll 2\pi c/a$. Thus in addition to Eq. (2), the conditions

$$a \ll D, \quad a \ll L \tag{3}$$

must be satisfied in order to provide $\varepsilon_{\mathrm{eff}} \approx \mathrm{const}$. Here $L$ and $D$ are the period and thickness of the PS, respectively. In the following, we always assume that both Eqs. (2) and (3) are satisfied and that $\omega_{\mathrm{cut}} \propto 2\pi c/D \propto 2\pi c/L$.

The first two time-harmonic Maxwell equations in the bounded source-free ULPM medium with $\mathrm{Re}\{\varepsilon\} = 0$ and $\mathrm{Im}\{\varepsilon\} = \varsigma$, $0 \leqslant \varsigma \ll 1$ are

$$\vec{\nabla} \times \vec{E} = i\omega\mu\mu_0 \vec{H}, \tag{4}$$

$$\vec{\nabla} \times \vec{H} = \omega\varsigma\varepsilon_0 \vec{E}, \tag{5}$$

and the Helmholtz equations for the electric and magnetic field read

$$\vec{\nabla}^2 \vec{E} = -i\varsigma\mu k^2 \vec{E}, \tag{6}$$

$$\vec{\nabla}^2 \vec{H} = -i\varsigma\mu k^2 \vec{H}. \tag{7}$$

In Eqs. (4)–(7), $\varepsilon_0$, $\mu_0$, and $k = \omega/c$ are the free-space permittivity, permeability, and wave number, respectively.

The right-hand sides of Eqs. (5)–(7) are responsible for the extent to which the fields differ from static ones. In the lossless case, i.e., $\varsigma = 0$, Eqs. (6) and (7) are reduced to

$$\vec{\nabla}^2 \vec{E} = 0, \tag{8}$$

$$\vec{\nabla}^2 \vec{H} = 0. \tag{9}$$

Thus the total electromagnetic field within a ZPM medium behaves in this case like a superposition of an electrostatic electric and a magnetostatic magnetic field. Introducing currents inside the slab, i.e., replacing 0 with $-\vec{\nabla} \times \vec{J}$ in Eq. (9),

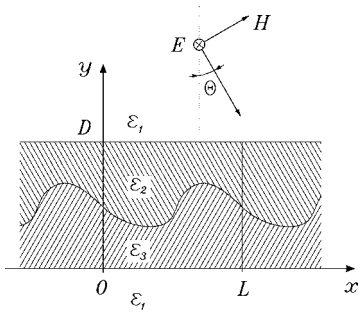


FIG. 1. Geometry of the scattering problem.

setting $\mu=0$ in Eq. (4), and replacing the right-hand side of Eq. (5) with $\vec{J}$, one obtains the case considered in Ref. 11.

When an *s*-polarized wave is incident from the air (upper) half-space on a periodically corrugated interface of the ZPM (lower) half-space, the total field below the interface, i.e., at $y<0$, which satisfies Eqs. (6) and (7), can be expressed as

$$E(x,y)=\sum_{n=-\infty}^{\infty}\tau_n\exp(i\alpha_n x-i\eta_n y), \tag{10}$$

where $\eta_n=\sqrt{i\varsigma\mu k^2-\alpha_n^2}$, $\mathrm{Im}\{\eta_n\}\geqslant 0$, $\alpha_n=\alpha_0+2\pi n/L$, $\alpha_0=k\sin\theta$, and $\theta$ is the angle of incidence. In the lossless case, $\eta_n=i|\alpha_n|$ and the *y*-dependent term in Eq. (10) is reduced to $\xi_n=\exp(|\alpha_n|y)$, so that any mode in the series over *n* becomes evanescent, except for the case with $\alpha_n=0$ leading to $\xi_n=1$. If $k\neq 0$, this situation occurs at $kL\sin\theta=-2\pi n$ corresponding to the $(-2n)$th Bragg angle. In particular, it is realized at $\theta=n=0$. For a mode with $n=0$ and arbitrary $\theta$, $\xi_n=\exp(|\alpha_0|y)$, which will vanish with increasing $|\alpha_0|$ and $|y|$. If $\varsigma>0$, $\mathrm{Re}\{\eta_n\}\neq 0$ and $\mathrm{Im}\{\eta_n\}\neq 0$ simultaneously.

Despite that the modes in the ZPM are evanescent in most cases, a significant portion of the energy of the incident wave can tunnel through a rather thin slab of such a medium so that an exponential decrease of $\mathcal{T}$ occurs with increasing $k$ and/or $\theta$ leading to a cutoff-type behavior. In the case of a noncorrugated homogeneous ZPM slab, this effect can be observed using the above mentioned standard formulas for reflection/transmission. In the case of a corrugated periodic ZPM slab, such a behavior is expected to appear in the multimode regime, too, while the exponential decrease depends on *n*.

In this paper, we consider two types of structures. In Fig. 1, a PS of the second type is shown, which will further be referred to as PSII. A PS of the first type (PSI) is easily obtained from PSII by setting $\varepsilon_2=\varepsilon_1$. We assume that $\mu=1$, $\varepsilon_1=1$, and that an incident electromagnetic wave propagates in the direction of negative *y*,

$$E^i(x,y)=E_0^i\exp(i\alpha_0 x-i\beta_0 y), \tag{11}$$

where $\beta_0=k\cos\theta$. The corrugated boundary is given by

$$h(x)=h_0+h_1\sin(2\pi x/L), \tag{12}$$

with $h_0-h_1\geqslant 0$ and $h_0+h_1\leqslant D$, so that the corrugation depth $d=2h_1$.

To solve the scattering problem, we apply the recently developed fast coupled-integral-equations technique.[28] It is based on the standard volume electric field integral equation, which reads within $0\leqslant y\leqslant D$,

$$E^i(x,y)=E(x,y)-k^2\int_0^D\int_{-\infty}^{\infty}G(x-x',y-y')\times\chi(x',y')E(x',y')\mathrm{d}x'\mathrm{d}y', \tag{13}$$

where $E$ is the total field, which must be solved for. The kernel of the convolution integral is given by the free-space Green's function $G(x,y)=(i/4)H_0^{(2)}[k\sqrt{x^2+y^2}]$, where $H_0^{(2)}$ denotes the Hankel function of the second-kind and $\chi(x,y)=\tilde{\varepsilon}(x,y)-1$, with $\tilde{\varepsilon}=\varepsilon_2$ for $h(x)<y<D$ and $\tilde{\varepsilon}=\varepsilon_3$ for $0<y\leqslant h(x)$.

As $\chi$ is periodic in the $x$ direction, we expand it into a Fourier series

$$\chi(x,y)=\sum_{m=-\infty}^{\infty}\chi_m(y)\exp(iv_m x), \tag{14}$$

where $v_m=2\pi m/L$ and the expansion coefficients are given by

$$\chi_m(y)=\frac{1}{L}\int_0^L\chi(x,y)\exp(-iv_m x)\mathrm{d}x. \tag{15}$$

Since the total field is pseudoperiodic, it can also be expanded into a series

$$E(x,y)=\sum_{n=-\infty}^{\infty}E_n(y)\exp(i\alpha_n x), \tag{16}$$

where $\alpha_n=\alpha_0+v_n$. Substituting of Eqs. (15) and (16) into Eq. (13), we obtain after some straightforward manipulations the following coupled integral equations:

$$E_0^i\exp(-i\beta_0 y)\delta_{m0}=E_m(y)+\frac{k^2}{2i\beta_m}\sum_{n=-\infty}^{\infty}\int_0^D\exp(i\beta_m|y-y'|)\chi_{m-n}(y')\times E_n(y')\mathrm{d}y',\quad y\in[0,D],\ m=0,\pm 1,\pm 2,\ldots, \tag{17}$$

where $\beta_m=\sqrt{k^2-\alpha_m^2}$ with $\mathrm{Im}\{\beta_m\}\geqslant 0$ and $\delta_{m0}$ denote the propagation constant and the Kronecker delta, respectively. Further, the values of $\omega$ and $\theta$ corresponding to the Rayleigh wavelengths, i.e., to $\beta_m=0$, are denoted by $\nu_m$ and $\varphi_m$, respectively. The fast method which has been applied to solve Eq. (17) is described in Ref. 28.

Once the field distribution within the region $0\leqslant x\leqslant L$, $0\leqslant y\leqslant D$ is found, the Fourier amplitudes $\rho_n$ and $\tau_n$ of modes (Bragg beams) $R_n$ in the upper half-space and $T_n$ in the lower one are calculated as

$$\rho_n=E_n(D)-\delta_{n0}E_0^i, \tag{18}$$

$$\tau_n = E_n(0). \tag{19}$$

Furthermore, we use DEs in order to characterize the energy distribution between the modes, which is the most important characteristic of the far field of any PS. According to the conventional definition,[33] reflection ($r_n$) and transmission ($t_n$) DEs are equal to a part of the total energy in the reflected $R_n$ and transmitted $T_n$ propagating modes, respectively. Hence they can be written as follows:

$$r_n = \mathrm{Re}\{\beta_n \rho_n \rho_n^*/\mathcal{W}\}, \tag{20}$$

$$t_n = \mathrm{Re}\{\beta_n \tau_n \tau_n^*/\mathcal{W}\}, \tag{21}$$

where $\mathcal{W}$ is the energy of the incident wave and the asterisk means complex conjugation. In a lossless case, the sum of all DE values must be unity if $\mathcal{W}=1$, i.e.,

$$\mathcal{R} + \mathcal{T} = 1, \tag{22}$$

where $\mathcal{R}=\Sigma_{n=-\infty}^{\infty} r_n$ and $\mathcal{T}=\Sigma_{n=-\infty}^{\infty} t_n$.

For calculations of $\omega$ dependencies of $r_n$ and $t_n$, we assume that $\mathrm{Re}\{\varepsilon_{\mathrm{eff}}\}=\mathrm{const}$, keeping in mind, however, that any two values of $\omega$ correspond, in fact, to two different realistic materials. At the same time, no such restriction is required when the $\theta$ dependence of the DE is considered at fixed $\omega$, provided that Eqs. (2) and (3) are valid.

## III. NUMERICAL RESULTS AND DISCUSSION

### A. Periodic structure I: Frequency dependence

We consider now several examples, which demonstrate basic effects arising in scattering by a PSI. A part of these effects is illustrated by Fig. 2, where DE values corresponding to (a) all and (b) most of the propagating modes are shown in the case of an intermediate thickness. One of these effects manifests itself in the suppression of higher propagating modes ($|n|>0$) in transmission, while the contribution of the higher modes to reflection remains significant. In Fig. 2(a), only $T_0$ contributes substantially to $\mathcal{T}$, although $T_{-1}$ and $T_{-2}$ are propagating, too. Hence the number of really contributive modes $T_n$ can be *less* than that of formally propagating modes. This effect appears due to the ZPM. It is close to the effect of wavefront straightening observed for the matched zero-index medium in Ref. 11.

It is known that in case of a finite-thickness dielectric grating, a larger $\varepsilon=\varepsilon_3$ results in a larger number of modes propagating and hence in a more complicated structure of the field lines inside the dielectric. Decrease of $\varepsilon$ leads to a smaller number of propagating modes and to a static field in the limiting case of $\varepsilon_3=0$. An illustrative example of a near-field pattern, which is typical in that a strong effect of the corrugation above the upper interface and a straightened field at the lower one are observed, is depicted in Fig. 3 for the case that $kL=3.8$ as in Fig. 2(a). As the result, the field structure above PSI becomes more complicated than below it, leading to a larger number of really contributive modes in reflection than in transmission.

The second important effect originating from zero permittivity is the cutoff-type behavior of $\mathcal{T}$ and $t_0$, which is seen in

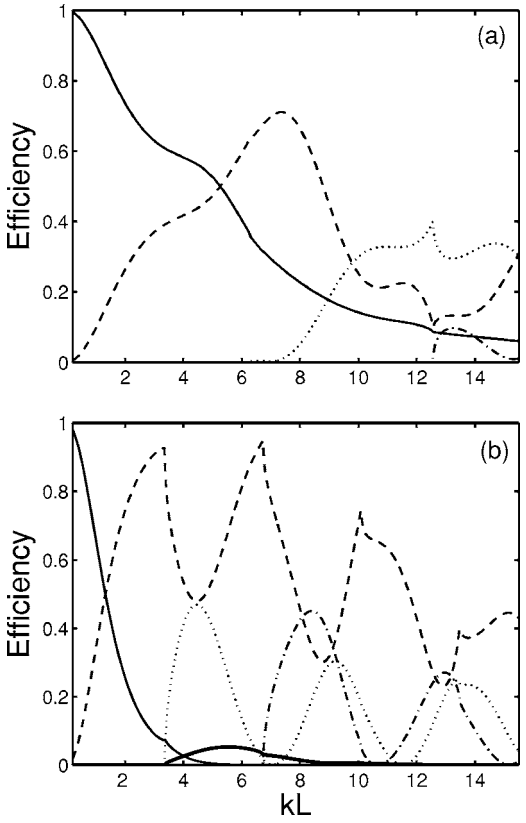


FIG. 2. Frequency dependence of DE for a PSI at (a) $\theta=0$ and (b) $\theta=\pi/3$; $D/L=1$, $h_0=0.68$, $h_1=0.32$, $\varepsilon_2=1$, and $\varepsilon_3=0$. Solid, dashed, thick solid, dotted, and dashed-dotted lines show $t_0$, $r_0$, $t_{-1}$, $r_{-1}$, and $r_{-2}$, respectively, which correspond to the most contributive modes; $t_{-2}\approx 0$ for $k>\alpha_{-2}$. At $\theta=0$, $r_n=r_{-n}$, $t_n=t_{-n}$, and $t_{-1}\approx 0$ for $k>\alpha_{-1}$.

Fig. 2(b). Here $t_0$ exponentially decreases and takes almost-zero values at $kL>5.5$, while $\mathcal{T}$ does so at $kL>8.5$. These effects appear despite the fact that $T_0$, $T_{-1}$, and $T_{-2}$ are allowed to propagate starting from the same $kL$ values as $R_0$, $R_{-1}$, and $R_{-2}$, respectively. An increase of $\theta$ leads to shifting the cut-off towards smaller $kL$ values and to nonzero contri-

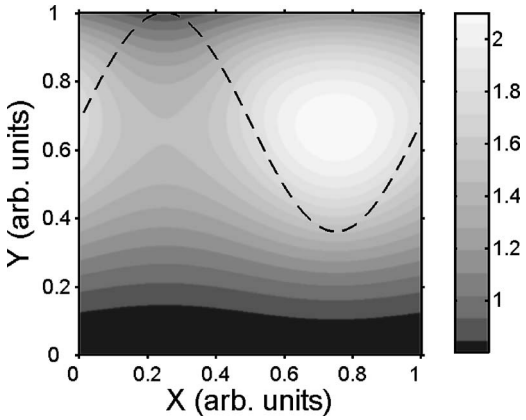


FIG. 3. Electric field pattern within the region $0\leqslant x\leqslant L$, $0\leqslant y\leqslant D$ for $kL=3.8$ and the same other parameters as in Fig. 2(a). In this case, $\mathcal{R}=0.41$ and $\mathcal{T}=0.59$. The ZPM-dielectric interface is shown by a dashed line.

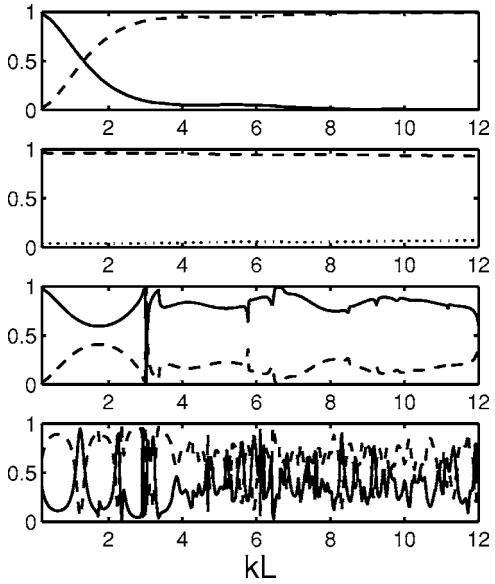


FIG. 4. Comparison of transmittance (solid lines) and reflectance (dashed line) for four structures with $\varepsilon_3=0$ (most upper subplot), $\varepsilon_3=(1.3+i7.6)^2$ (second upper subplot), $\varepsilon_3=2.1$ (third upper subplot), and $\varepsilon_3=11.4$ (lowest subplot), at the same geometrical parameters and $\theta$ as in Fig. 2(b). For the second upper subplot, absorption $\mathcal{A}=1-\mathcal{R}-\mathcal{T}$ is shown by the dotted line.

bution of some modes $T_n$ at $|n|>0$. For the parameters of Fig. 2(a), cut-offs of $\mathcal{T}$ and $t_0$ take place at $kL>16$.

It follows from the obtained results that a possibility should exist to redirect a part of the energy to the upper and lower half-spaces depending on $\omega$, while a part of formally propagating modes is suppressed, and hence an overmoding is avoided. For example, in Fig. 2(b), $r_0=t_0$ at $kL=1.325$ while higher modes in the air half-spaces are still evanescent, and $r_0\approx r_{-1}$ at $kL=4.45$ while only modes $R_{-1}$ and $R_0$ are substantially contributive, so that the case of two dominating, equally contributive modes can be realized in PSI in both single ($k<\alpha_{-1}$) and multimode ($k>\alpha_{-1}$) regimes.

A PSI shows in some sense intermediate behavior between structures of the same geometry either made of pure metal or of pure dielectric. For the metallic PS, the transmitted field vanishes; the dielectric PS is usually characterized by either a prevalence of transmission (small $\varepsilon_3$, e.g., $\varepsilon_3=2.1$) or a competition of transmission and reflection (large $\varepsilon_3$, e.g., $\varepsilon_3=11.4$) (see Fig. 4). Although mode competition occurs in the case of a dielectric, what can lead to prevailing of a certain mode in transmission, not all these modes disappear starting from some $kL$. This is the main difference between the cases with $\varepsilon_3=0$ and $\varepsilon_3=11.4$. PSI behaves like a dielectric grating with rather small $\varepsilon_3$ at small $kL$, and like a metallic one at rather large $kL$. Note that the cutoff-type behavior of $t_0$, which is similar to that seen in Fig. 2, had also been observed for multilayer grid structures with capacitive metallic constituents of resonance size elsewhere.[33]

An increase of $D/L$ results, as compared to Fig. 2, in reflection dominating over transmission starting from a smaller $kL$. An example is shown in Fig. 5, where $D/L=1.5$ and $d/L=0.96$. In this case, $\mathcal{R}>0.99$ starting from $kL\approx 7.5$. Besides, the extrema are enhanced and $r_0$ approaches unity at certain conditions. In this regime, the near-zone field shows a maximum at $y>h(x)$ (in a similar manner as in Fig. 3), which is typical for vacuum modes.

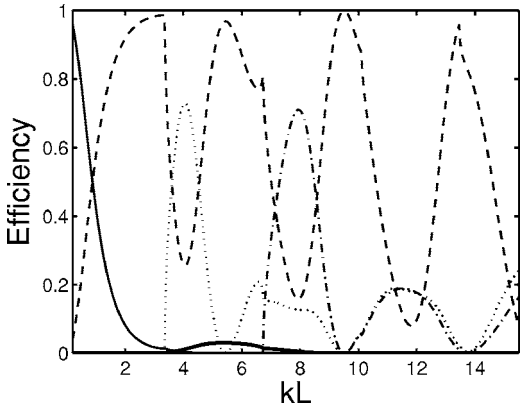


FIG. 5. Same as Fig. 2(b), but for $D/L=1.5$.

A decrease of $D/L$ leads to an increasing contribution of the modes $T_n$ with $|n|>0$, and to a shift of the cutoff effect towards larger $kL$. Hence the structure must be thick enough in order to let the effects described above be well pronounced. On the other hand, an increase of $D/L$ can lead to a substantial increase of the losses if $\mathrm{Im}\{\varepsilon_{\mathrm{eff}}\}\neq 0$. Hence it must be thin enough in order to keep the losses at a reasonable level.

An introduction of rather small losses does not lead to any qualitative change in the relative contribution of the separate modes, as well as in the behavior of $r_n$ and $t_n$ vs $kL$. However, the regime of (almost) total reflection disappears now. These features are illustrated in Fig. 6 for the same parameters as in Fig. 5, except for $\mathrm{Im}\{\varepsilon_{\mathrm{eff}}\}$. At the parameters of Fig. 6, absorption $\mathcal{A}$ varies from 0.065 to 0.19 at $\mathrm{Im}\{\varepsilon_{\mathrm{eff}}\}=0.045$ and from 0.022 to 0.07 at $\mathrm{Im}\{\varepsilon_{\mathrm{eff}}\}=0.015$ while $kL$ varies from 2 to 10. At $h_0=0.68$, $h_1=0.32$, $D/L=0.5$ and the same $kL$, $\mathcal{A}$ does not exceed 0.088 at $\mathrm{Im}\{\varepsilon_{\mathrm{eff}}\}=0.045$ and 0.031 at $\mathrm{Im}\{\varepsilon_{\mathrm{eff}}\}=0.015$. Note also, that no unusual behavior of the DE values corresponding to $\xi_n=1$ is revealed. The same holds true for most of the cases considered in the next sections.

### B. Periodic structure II: Frequency dependence

In this section, we emphasize on the effects which appear due to adding a complementary dielectric layer to the ZPM

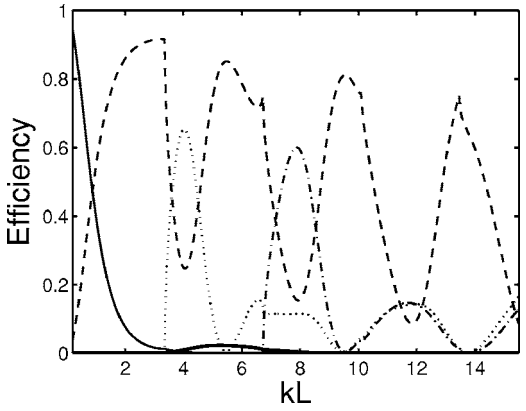


FIG. 6. Same as Fig. 5, but for $\mathrm{Im}\{\varepsilon_3\}=0.045$.

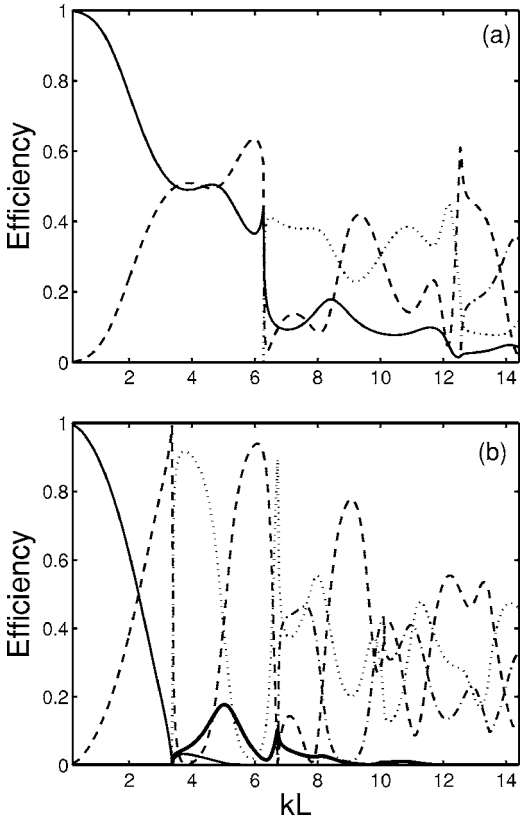


FIG. 7. Frequency dependence of DE for a PSII with intermediate thickness at (a) $\theta=0$ and (b) $\theta=\pi/3$; $\varepsilon_2=2.1$, $\varepsilon_3=0$. The geometrical parameters are the same as in Fig. 2. Solid, dashed, thick solid, dotted, and dashed-dotted lines correspond to $t_0$, $r_0$, $t_{-1}$, $r_{-1}$, and $r_{-2}$, respectively. In case (a), $t_{-1}\approx 0$ at $k>\alpha_{-1}$, $t_{-2}\approx 0$ at $k>\alpha_{-2}$, $t_n=t_{-n}$, and $r_n=r_{-n}$.

one. A variety of interesting diffraction effects is known for finite-thickness gratings with dielectric constituents, which are mostly due to a larger number of propagating modes in the dielectric than in the air half-spaces. This leads to the appearance of regimes of bulk and surface modes, whose particular manifestations are also called "forced surface modes" and "trapped modes."[34] Such effects like total reflection and neighboring reflection and transmission peaks are associated with them.

In line with the so-called two-channel condition, at least two modes with different propagation constants must be propagating between the half-spaces (i.e., at least two channels for energy exchange must be open), in order to obtain a total reflection effect.[34] In our case, there is no propagating mode in the ZPM layer, while in the dielectric more than one mode can be propagating. This occurs if

$$\omega > \Omega_{-1}, \tag{23}$$

where $\Omega_{-1}$ corresponds to $(\Omega_{-1}/c)^2\varepsilon_2-\alpha_{-1}^2=0$.

Our consideration is restricted to the case of $\varepsilon_2=2.1$. An illustrative example is presented in Fig. 7. One can see that suppression of higher modes in transmission, which are allowed to propagate, and a cut-off in $t_0$ and $\mathcal{T}$ are common features for both PSI and PSII. From a comparison of Figs. 2 and 7, the features arising from adding the dielectric layer are clearly seen. In particular, the zones of slight variations (plateaus) of $r_n$ and $t_n$, and the switching between the modes at $\omega\approx\nu_n$ do appear. The frequency range, at which the latter effect occurs, can be combined with that of the $t_0$ cut-off. The effect of higher modes is usually stronger for PSII.

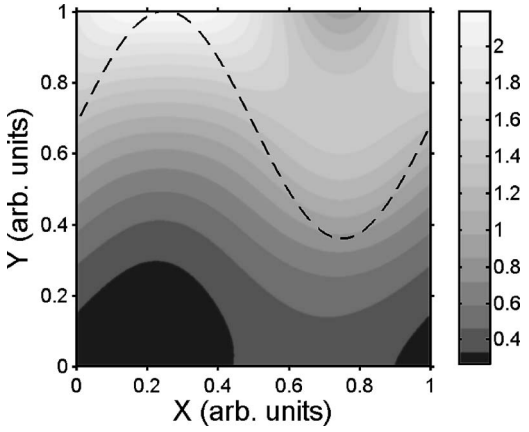


FIG. 8. Electric field pattern within the region $0\leqslant x\leqslant L$, $0\leqslant y\leqslant D$ corresponding to a reflection peak at $kL=3.365$ in Fig. 7(b). The ZPM-dielectric interface is shown by the dashed line.

A regime with $r_0>0.99$ appears in Fig. 7(b) at $kL=3.365$ while two modes propagate in the dielectric at $h(x)<y<D$ and $\nu_{-1}L/c=3.367$. It can be interpreted either as a maximum of $r_0$ of PSI, which is enhanced and slightly shifted by a dielectric, or as a shift of the maximum of $r_0$ of a dielectric structure with the same parameters as in Fig. 7(b), except for $\varepsilon_3=1$, by a ZPM layer. For PSI, a maximum of $r_0=0.927$ occurs at $kL=3.324$. For the dielectric structure, $r_0=1$ at $kL=3.218$. Contrary to the mentioned maximum in Fig. 2(b), a surface-mode-type behavior of the field occurs in this regime, while an evanescent mode shows maximal amplitude, $|\rho_{-1}|/|\rho_0|\approx 1.64$ (see Fig. 8).

The enhancement of the effects caused by an increase of the relative volume which is occupied by the dielectric is illustrated in Fig. 9. In particular, one can see the narrow peak of $r_0=1$ which arises at $kL=5.955$, i.e., in the vicinity of $\nu_{-1}L/c=2\pi$. Such a behavior is typical for dielectric gratings. It can be interpreted rather as a shift of the maximum of $r_0=1$, which appears for a grating with $\varepsilon_2=2.1$ and $\varepsilon_3=1$ at $kL=5.378$ (PSI shows a maximum $r_0=0.289$ at $kL=6.265$). Hence an interpretation of this effect as a peak shifting towards $kL=\nu_{-1}L/c$ when adding a ZPM layer is more flexible.

In the case of the peak in Fig. 9, $|\rho_{\pm 1}|/|\rho_0|\approx 2.7$, while the $\pm 1$th modes are propagating in the dielectric, but are evanescent in air. As a result, the field is mostly concentrated within the dielectric (see Fig. 10). Hence this regime is formally belonging to the bulk modes. It is seen from Figs. 8 and 10 that in an (almost) total reflection regime, the region of the strongest field localization depends on the location of the ZPM-dielectric interface and that of the dielectric-air interface with respect to each other. Note that although the field is still far from zero within the ZPM layer at $y=0$, it is coupled only to evanescent modes of the lower half-space.

From the results obtained it follows that a switching effect occurs, if Eq. (23) is satisfied. The same remains true with

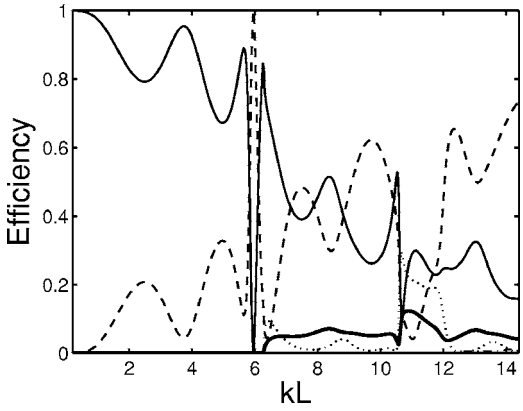


FIG. 9. Demonstration of the effect of decreasing the thickness of the ZPM layer for PSII: $h_0=0.5$, $h_1=0.4$, $D/L=1$, $\varepsilon_2=2.1$, $\varepsilon_3=0$, and $\theta=0$. Solid, dashed, thick solid, dotted, and dashed-dotted lines correspond to $t_0$, $r_0$, $t_{-1}$, $r_{-1}$, and $r_{-2}$, respectively; $t_n=t_{-n}$ and $r_n=r_{-n}$.

respect to the sharp peaks observed. On the other hand, the plateaus can correspond partially to $\omega<\Omega_{-1}$ and partially to $\omega>\Omega_{-1}$.

Varying $D/L$, $h_0$, and $h_1$, one can realize a part of the above-described effects in a desired combination. Most of these effects also exist, if losses due to $\mathrm{Im}\{\varepsilon_3\}>0$ are taken into account. This usually leads to quantitative differences only, which are increasing with $kL$ and $D/L$. A sample dependence of $\mathcal{A}$ vs $kL$ is depicted in Fig. 11. In comparison to a PSI, sharp extrema are observed at $\omega=\nu_n$, provided that $D/L$ is large enough. It is worth noting a nonmonotonous behavior of $\mathcal{A}$ vs $D/L$, which has not been observed for PSI. However, the typical values of $\mathcal{A}$ and its trend to grow in average with $kL$ are the same.

### C. Periodic structure I: Angular dependence

It follows from Snell's Law[30] that when a light beam is incident from a high-index to a low-index material, and $\theta$ exceeds a certain threshold, total reflection occurs. In Fig. 12, this effect is demonstrated for a noncorrugated ZPM slab and for a PSI with the same parameters as in Fig. 2. For a PSI, angular cut-off takes place in both single- and multimode regimes. Other effects found at varying $kL$ also have their analogs at varying $\theta$.

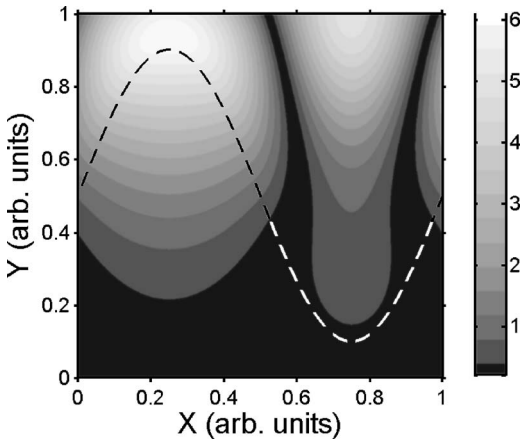


FIG. 10. Electric field pattern within region $0\leqslant x\leqslant L$, $0\leqslant y\leqslant D$ corresponding to a reflection peak at $kL=5.955$ in Fig. 9. The ZPM-dielectric interface is shown by the dashed line.

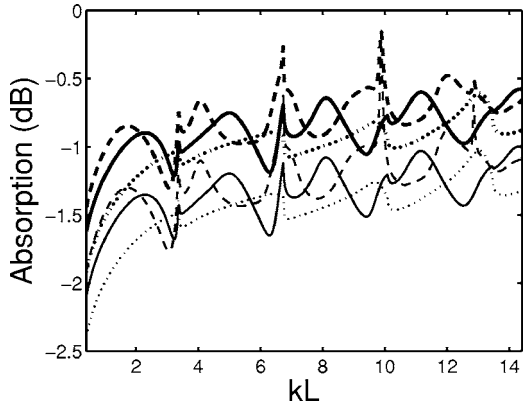


FIG. 11. Absorption vs $kL$. Thin lines, $\mathrm{Im}\{\varepsilon_3\}=0.015$; thick lines, $\mathrm{Im}\{\varepsilon_3\}=0.045$. Solid, dashed, and dotted lines correspond to $D/L=1.0$, $D/L=1.5$, and $D/L=0.5$, respectively; $h_0=0.68$, $h_1=0.32$, and $\theta=\pi/3$.

Figure 13 demonstrates the angular cut-off in $t_0$, and the suppression of $T_{-1}$, a propagating mode. It is worth noting that in order to obtain these effects, the structure should carefully be designed. Indeed, if $kL$ is too small, cut-off can be realized only in the vicinity of $\theta\approx\pi/2$. If $kL$ is too large, $t_0$ can be very small even at $\theta=0$, and furthermore at larger $\theta$. It follows from the obtained results that *a necessary condition* for the appearance of angular cut-offs of $\mathcal{T}$ and $t_0$ within a certain range, $\theta_l<\theta<\theta_u$, is that $kL$ belongs to a range of values, which are smaller than those associated with the frequency cut-off at $\theta_l$ and larger than those at $\theta_u$.

On the other hand, an increase of $D/L$ simultaneously leads to a decrease of the $t_0$ value at $\theta=0$ and to a decrease of the ratios $\max\{t_n\}/\max\{t_0\}$, $n=-1,-2,\ldots$. As a result, the

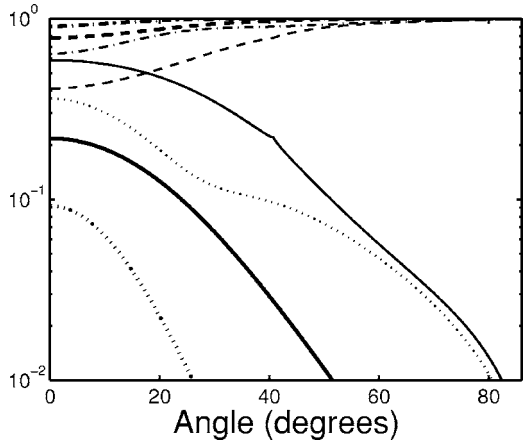


FIG. 12. Angular dependencies of $\mathcal{T}$ and $\mathcal{R}$ for PSI with $D/L=1.0$, $h_0=0.68$, and $h_1=0.32$ (thin lines) and a noncorrugated ZPM slab with $h_0=1.0$ and $h_1=0$ (thick lines); solid, dashed, dotted, and dashed-dotted lines correspond to $\mathcal{T}$ and $\mathcal{R}$ at $kD=3.8$, and $\mathcal{T}$ and $\mathcal{R}$ at $kD=2\pi$, respectively.

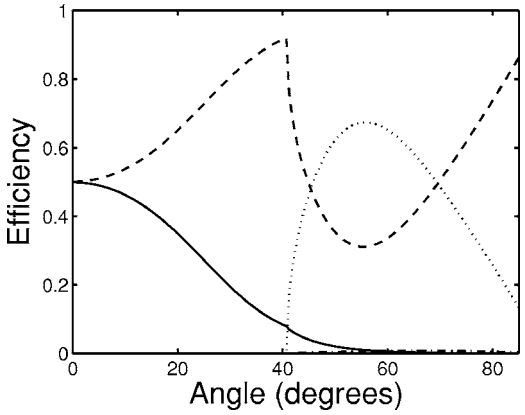


FIG. 13. Angular dependence of DE for a PSI with $h_0=0.68$, $h_1=0.32$, $D/L=1.5$, and $kL=3.8$. Solid, dashed, dashed-dotted, and dotted lines correspond to $t_0$, $r_0$, $t_{-1}$, and $r_{-1}$, respectively.

contribution of the transmittance to the total energy and the contribution of the higher modes to the transmission become weaker. Hence the $D/L$ value should be large enough in order to suppress the higher modes and to obtain cut-off at intermediate $\theta$, but it should be small enough in order to let the transmittance be not (almost) zero at least at $\theta=0$.

If $\mathrm{Im}\{\beta_{-1}\}=0$ for all values of $\theta$ from 0 to $\pi/2$, it is not realistic to obtain cut-offs for all propagating modes in transmission rather far from $\theta=\pi/2$, and furthermore to suppress all higher modes simultaneously with a significant value of $t_0$ at small $\theta$. The thickness needed to realize the former is usually too large to realize the latter. The case when only the modes with $n=0$ propagate at small $\theta$ and only with $n=0$ and $-1$ at large $\theta$, as in Fig. 13, seems to be most interesting from the point of view of the appearance of both cut-off and suppression effects.

Note that in Fig. 13, $r_0=t_0=0.5$ at $\theta=0°$ and $r_0=r_{-1}\approx 0.5$ at $\theta=70°$. At $h_0=0.5$, $h_1=0.4$ and the same other parameters as above, $r_0=t_0=0.5$ at $\theta=35°$ and $r_0=r_{-1}\approx 0.5$ at $\theta=72°$. Hence an equal contribution of the desired modes can be obtained for two $\theta$-values simultaneously. Thus the PS of this type can effectively be used for a redistribution of the energy between the reflectance and transmittance and between separate modes, depending on $\theta$.

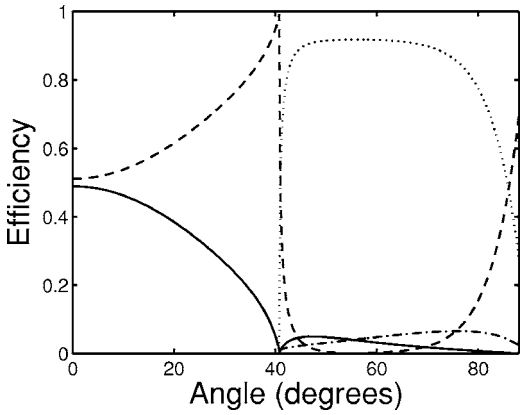


FIG. 14. Angular dependence of DE for a PSII with $D/L=1.0$, $\varepsilon_2=2.1$, $\varepsilon_3=0$, $h_0=0.68$, and $h_1=0.32$, at $kL=3.8$. Solid, dashed, dashed-dotted, and dotted lines correspond to $t_0$, $r_0$, $t_{-1}$, and $r_{-1}$, respectively.

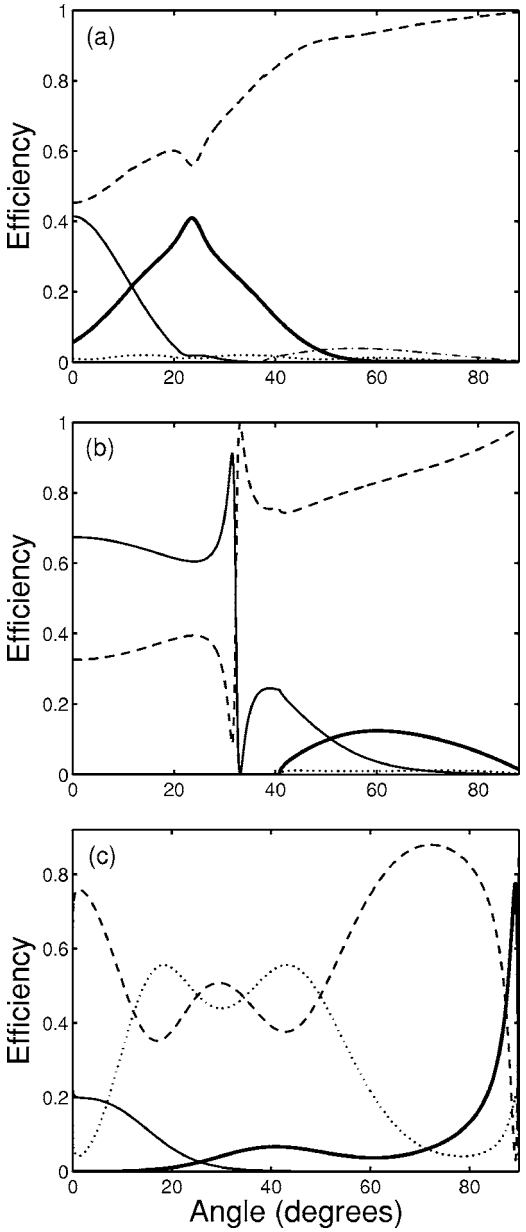


FIG. 15. Demonstrating abnormal effects arising due to the ZPM layer at $\varepsilon_2=2.1$, $\varepsilon_3=0$: (a) $D/L=1.0$, $h_0=0.5$, $h_1=0.4$, and $kL=7.8$; (b) $D/L=1.5$, $h_0=0.5$, $h_1=0.4$, and $kL=3.8$; (c) $D/L=1.5$, $h_0=0.68$, $h_1=0.32$, and $kL=2\pi$. Solid, dashed, thick solid, and dotted lines correspond to $t_0$, $r_0$, $t_{-1}$, and $r_{-1}$, respectively. In case (a), $r_{-2}$ is shown by a dashed-dotted line.

### D. Periodic structure II: Angular dependence

Similarity of the effects occurring in the frequency and angular dependencies of the DE is also present for PSII. In Fig. 14, several effects are observed, including a cutoff-type behavior of $t_0$ and various scenarios of the switching between different modes. A regime with $r_0$ approaching unity appears at $\psi_{-1}<\theta\approx\varphi_{-1}$ where $\psi_{-1}$ corresponds to the Ray-

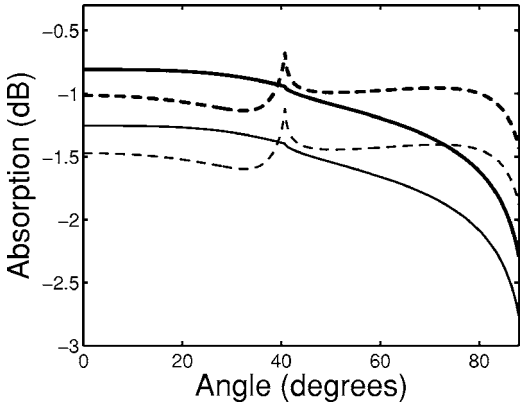


FIG. 16. Comparison of the angular dependencies of the absorption for a PSI (solid lines) and a PSII (dashed lines) at $kL=3.8$, $D/L=1.0$, $h_0=0.68$, and $h_1=0.32$. Thin and thick lines correspond to $\mathrm{Im}\{\varepsilon_3\}=0.015$ and 0.045, respectively.

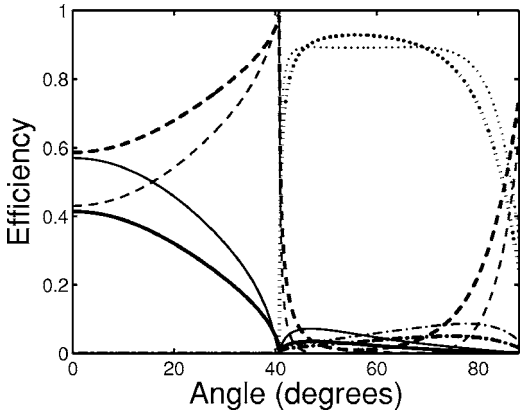


FIG. 17. Demonstration of the effect of $\varepsilon_3$ in the vicinity of zero: thick lines—$\varepsilon_3=-0.1$, thin lines—$\varepsilon_3=0.1$, the other parameters are the same as in Fig. 14. Solid, dashed, dotted, and dashed-dotted lines correspond to $t_0$, $r_0$, $r_{-1}$, and $t_{-1}$, respectively.

leigh wavelength of the $-1$th mode in the dielectric. The roles played here by both the dielectric and the ZPM layers are the same as in such a regime in Fig. 7(b). Although cut-offs of $t_0$ and $t_{-1}$ are realized for the used parameters only in the vicinity of $\theta=\pi/2$, these effects can be obtained in a more pronounced form at intermediate $\theta$ by increasing $D/L$.

An increase of $kL$ leads to the enhancing role of higher modes in transmission and to a larger number of combinations of simultaneously arising effects as well. The results obtained show that the condition

$$\theta > \psi_{-1}, \tag{24}$$

plays the same role as Eq. (23) for the appearance of the dielectric-related effects in PSII.

We consider now several examples of *an abnormal behavior* of the DE values vs $\theta$, which appears due to the combination of a ZPM and a dielectric layer. They are shown in Fig. 15. In case (a), all-angle suppression of higher reflective modes $R_n$, $|n|>0$ takes place, while $t_0$ and $t_{-1}$ show cut-offs and rather large and close to each other maximal values. Note, that in this case, $|\rho_1|\approx|\rho_0|>|\tau_{-1}|$ at the maximum of $t_{-1}$. In case (b), the switching between $T_0$ and $R_0$ occurs at $\psi_{-1}<\theta<\varphi_{-1}$ leading to the neighboring peaks of $r_0\approx 1.0$ and $t_0\approx 0.9$. Both of them are accompanied by a rather strong bulk mode, while $|\rho_{-1}|=\max\{|\rho_n|,|\tau_n|\}_{n=-\infty}^{\infty}$. At $\theta>\varphi_{-1}$, $R_{-1}$ is suppressed.

In Fig. 15(c), one can see sharp maxima of $\mathcal{T}$ and $t_{-1}$ arising at $\theta=\theta_{\max}=\pi/2-u$, $u\ll\pi/2$. At $\theta_{\max}<\theta<\varphi_{-2}=\pi/2$, $\mathcal{T}$ and $t_{-1}$ fall down to zero, so that $\mathcal{R}$ tends to unity in very close vicinity of $\theta=\pi/2$. The origin of the observed behavior is not yet understood satisfactorily. Most probably, it is either similar to the case of two neighboring peaks in Fig. 15(b) or related to the peculiarities in the appearance of a nonevanescent static field with $\xi=1$, which corresponds to $\theta=\pi/2$ being a Bragg angle in this case. Note that at $\theta=\theta_{\max}$, $|\rho_{-2}|=\max\{|\rho_n|,|\tau_n|\}_{n=-\infty}^{\infty}$.

The abnormal effects observed in Figs. 15(a) and 15(c) arise due to a combination of dielectric and ZPM layers, since they appear for neither PSI nor the dielectric structure with $\varepsilon_2=2.1$ and $\varepsilon_3=1$, while geometrical parameters are kept constant. For a part of the used range of $\theta$ variation, the suppression of $R_{-1}$ in Fig. 15(b) can be connected with the effect of the dielectric layer. However, the energy distribution between the modes in this case is substantially different from those in which either the PSI or the dielectric grating are present. In particular, for the dielectric structure two narrow peaks of $r_0=1$ are located at $\theta=25.9°$ and 40.2°. Once a ZPM layer is added to it, the two peaks will merge into one located at $\theta\approx 33°$, as shown in Fig. 15(b).

As in the case of PSI, an introduction of losses with $|\mathrm{Im}\{\varepsilon_3\}|<0.05$ does not result in a disappearance of any of the effects revealed. The only exception is related to the regime with $\mathcal{R}$ approaching unity. In Fig. 16, $\mathcal{A}$ vs $\theta$ is presented for PSI and PSII with the same geometrical parameters and $\mathrm{Re}\{\varepsilon_3\}$ as in Fig. 14. One can see that the presence of the dielectric at $h(x)<y<D$ allows one to decrease the losses within a wide range of $\theta$ variation. This range can be extended, e.g., by increasing $kL$. It is worth noting that the peaks of $\mathcal{A}$ do not necessarily appear. Usually they correspond to the sharp peaks of the $\theta$ dependencies of DEs in the vicinity of $\theta=\varphi_n$.

An increase of $\varepsilon_3$ from zero to unity results in a weaker contribution of higher modes. In turn, the effects found become weaker and disappear finally. On the other hand, there is no guarantee that these effects are strongest at $\varepsilon_3=0$. Hence varying $\varepsilon_3$ in the vicinity of zero promises to provide one with additional possibilities to control them. In Fig. 17, differences caused by changing the sign of $\varepsilon_3$ are illustrated in the lossless case. A comparison of Fig. 17 with Fig. 14 shows that all the main features remain. Furthermore, the presence and location of the regime with $r_0=1$ are not sensitive to the performed variation of $\varepsilon_3$, despite the above-discussed possible contribution of both the ULPM and the dielectric layers to the appearance of this effect.

## IV. CONCLUSIONS

In this paper, scattering of an *s*-polarized plane electromagnetic wave by a finite-thickness PS with sinusoidally

corrugated ULPM layer has been studied. The basic effects have been considered in detail. As was expected, scattering by such PS shows properties, which are in some sense intermediate to those of structures with the same geometry made of pure metal and of pure dielectric. Cutoff-type behavior of $t_0$ and $\mathcal{T}$ with increasing frequency and suppression of higher modes in transmission, which are formally propagating, are the basic effects for a PSI made of ZPM. In principle, these effects can be realized for a desired number of propagating modes. At frequencies which are smaller than cutoff, and for an appropriate choice of geometrical parameters, one more cutoff effect can appear, which manifests itself in decreasing and then vanishing $t_0$ and $\mathcal{T}$ at increasing $\theta$. The effects mentioned are rather related to the peculiar field distribution inside a ZPM, which is static for any frequency in the lossless case.

For PSII, the effects which arise due to the ZPM layer can be combined in a desired fashion with those due to the dielectric layer. The influence of these layers on each other can result in an enhancement/shift of some regimes related with one of the layers. A rich variety of combinations of the effects can be realized enabling new possibilities to control the number and amplitudes of the influential modes, and switching between various regimes depending on $\theta$. The possibility of an appearance of some effects caused by the presence of the dielectric can still be predicted by using the so-called two-channel condition, which is known from the studies of finite-thickness dielectric and metallo-dielectric gratings.

The thickness of a ZPM layer should be chosen taking into account two contradictive requirements. On the one hand, the presence of losses is a natural limitation imposed on the thickness. On the other hand, the detected effects caused by a ZPM require a rather large thickness of the layer in order to be pronounced. Several abnormal effects have been observed for PSII, which appear due to the combination of ZPM and dielectric layers. Their detailed investigation as well as a minimization of the losses is the subject of further studies. Variation of the metamaterial permittivity from positive to negative values in the vicinity of zero did not lead to any qualitatively new behavior compared to the case of ZPM. The effects studied can be used to extend the potentials of various optical and microwave technologies using frequency- and/or angular-selective components.

*Electronic address: serebryannikov@tu-harburg.de
†Presently with European Technology Center, Panasonic Electronic Devices Europe GmbH, D-21337 Lueneburg, Germany.
‡Presently with Katholieke Universiteit Leuven, B-3001 Leuven, Belgium.

[1] D. R. Smith, J. B. Pendry, and M. C. K. Wiltshire, Science **305**, 788 (2004).
[2] H. Chen, L. Ran, J. Huangfu, X. Zhang, K. Chen, T. M. Grzegorczyk, and J. A. Kong, J. Appl. Phys. **96**, 5338 (2004).
[3] K.-Y. Kim, IEEE Photonics Technol. Lett. **17**, 369 (2005).
[4] N. Garcia, E. V. Ponizovskaya, and J. Q. Xiao, Appl. Phys. Lett. **80**, 1120 (2002).
[5] C. Caloz, A. Sanada, and T. Itoh, IEEE Trans. Microwave Theory Tech. **52**, 980 (2004).
[6] L.-G. Wang, H. Chen, and S.-Y. Zhu, Phys. Rev. B **70**, 245102 (2004).
[7] A. Grbic and G. V. Eleftheriades, J. Appl. Phys. **92**, 5930 (2002).
[8] B. T. Schwartz and R. Piestun, Appl. Phys. Lett. **85**, 1 (2004).
[9] B. T. Schwartz and R. Piestun, J. Opt. Soc. Am. B **20**, 2448 (2003).
[10] R. W. Ziolkowski and C.-Y. Cheng, Radio Sci. **39**, RS2017 (2004).
[11] R. W. Ziolkowski, Phys. Rev. E **70**, 046608 (2004).
[12] A. Lakhtakia and T. G. Mackay, Microwave Opt. Technol. Lett. **41**, 165 (2004).
[13] K.-Y. Kim, Opt. Lett. **30**, 430 (2005).
[14] W. T. Lu and S. Sridhar, Microwave Opt. Technol. Lett. **39**, 282 (2003).
[15] S. Enoch, G. Tayeb, P. Sabouroux, N. Guerin, and P. Vincent, Phys. Rev. Lett. **89**, 213902 (2002).
[16] V. F. Rodríguez-Esquerre, M. Koshiba, H. E. Hernández-Figueroa, and C. E. Rubio-Mercedes, Appl. Phys. Lett. **87**, 91101 (2005).
[17] M. Schmidt, G. Boettger, M. Eich, W. Morgenroth, U. Huebner, R. Boucher, H. G. Meyer, D. Konjhodzic, H. Bretinger, and F. Marlow, Appl. Phys. Lett. **85**, 16 (2004).
[18] V. Kuzmiak and A. A. Maradudin, Phys. Rev. B **66**, 045116 (2002).
[19] R. Ruppin, Solid State Commun. **116**, 411 (2000).
[20] C. Li and Z. Chen, in *Progress in Electromagnetics Research*, edited by J. A. Kong (EMW, Cambridge, MA, 2003), Vol. 42, pp. 91–105.
[21] R. W. Ziolkowski and A. D. Kipple, IEEE Trans. Antennas Propag. **51**, 2626 (2003).
[22] R. A. Depine and A. Lakhtakia, Phys. Rev. E **69**, 057602 (2004).
[23] R. A. Depine, A. Lakhtakia, and D. R. Smith, Phys. Lett. A **337**, 155 (2005).
[24] A. Sihvola, *Electromagnetic Mixing Formulas and Applications* (IEE, London, 1999).
[25] M. I. Stockman, S. V. Faleev, and D. J. Bergman, Phys. Rev. Lett. **87**, 167401 (2001).
[26] J. Brown, Proc. IRE **100C**, 51 (1953).
[27] W. Rotman, IEEE Trans. Antennas Propag. **10**, 82 (1962).
[28] T. Magath and A. E. Serebryannikov, J. Opt. Soc. Am. A **22**, 2405 (2005).
[29] J. B. Pendry, A. J. Holden, W. J. Stewart, and I. Youngs, Phys. Rev. Lett. **76**, 4773 (1996).
[30] J. R. Reitz, F. J. Milford, and R. W. Christy, *Foundations of Electromagnetic Theory*, 4th ed. (Addison-Wesley, Reading, MA, 1993).
[31] W. C. Chew, *Waves and Fields in Inhomogeneous Media* (Van Nostrand Reinhold, New York, 1990).
[32] H. Cory and C. Zach, Microwave Opt. Technol. Lett. **40**, 461 (2004).
[33] *Electromagnetic Theory of Gratings*, edited by R. Petit (Springer-Verlag, Berlin, 1980).
[34] N. Amitay, V. Galindo, and C. P. Wu, *Theory and Analysis of Phased Array Antennas* (Wiley-Interscience, New York, 1972).